DESIGN AND FABRICATION OF SWITCH BASED BIO-INSPIRED AIRFLOW SENSORS

Bram Miller, Regan Kubicek, and Sarah Bergbreiter
Carnegie Mellon University, Pittsburgh, Pennsylvania, USA

ABSTRACT

Desert locusts possess an array of setae that function as aerodynamic sensors for flight stabilization. Using a similar sensing approach would be beneficial in ensuring a stable flight for micro-aerial vehicles, however implementation of current sensors is limited by size, information latency, and fabrication processes. This work focuses on the design and manufacturing of small bio-inspired airflow sensors to fulfill this role. This work introduces sensors that produce digital signals when subjected to a specific airflow threshold. The sensors are fabricated using a 3D printing microfabrication technique known as two-photon polymerization. This rapid manufacturing process allowed the fast production of sensors of varying flow sensitivity. The fabricated sensors showed high sensitivity to airflows below 5 m/s, and display behaviors like setae do in nature.

KEYWORDS

Bio-Inspired Sensing, Airflow Sensing, Switch-Based Sensing, Two-Photon Polymerization

INTRODUCTION

Micro-aerial vehicles (MAVs) have yet to achieve the same agility and stability found in small aerial insects. These insects, such as the desert locust *Schistocerca gregaria* and the hawkmoth *Manduca sexta,* possess a multitude of sensing modalities, such as vision, inertial, flow, and strain. Setae and their respective neural configurations provide information to insects significantly quicker than vision alone, allowing for more stable flight [1][2]. The goal of this work is to take inspiration from these sensing principles to develop quick and efficient airflow sensors for use in autonomous flight applications. We aim to develop arrays of flow sensors similar to the large banks of setae present on the head of desert locusts [2].

Setae are small, hairlike structures that protrude from the head of a locust and are used to sense external airflow [3] (Fig. 1). Flow is sensed when vibrations in the setae cause the sensory neuron to send regular trains of neural impulses to the insect through its central nervous system [3]. These setae function like digital switches by responding to a certain flow velocity threshold, and are often coupled together in strings of interneurons, condensing the neural data before passing it along to the final thoracic flight motor neurons [4]. Implementing arrays of digital airflow sensors like those found in the desert locust could allow MAVs to sense external disturbances in real time without the need of additional hardware, filtering, and software associated with traditional analog sensors.

The most common approach to sensing in aerial vehicles is the use of an inertial measurement unit, which can sense inertial disturbances based on the estimation of the current acceleration and rotational velocity of the aerial vehicle. However, when used on smaller MAVs, large inertial and aerodynamic disturbances may be detected too late to perform corrective maneuvers [5]. Piezoresistive MEMS sensors have previously been developed for airflow detection [6]. However, these sensors need to be continuously monitored and require additional hardware to manage signal amplification and filtering, which places further computational and hardware loads on limited MAV resources.

In this work we present a novel design for a bio-inspired airflow sensor (Fig. 2a). The sensor mechanism functions fundamentally like a push-button switch. When the designed airflow threshold is reached, the switch is closed and a current will flow. This design enables low-latency sensors capable of sending discrete signals without the need for continuous monitoring. Instead, a digital signal transitions from low to high, or high to low, at a designed flow threshold. By arraying these sensors and measuring the time between sensor activation, the flow velocity can be calculated and, when multi-directional sensors are applied, a flow direction can also be estimated. In this work, a static model is used to identify design parameters while calculating sensor thresholds. The sensors are fabricated using microscale 3D printing, sputter deposition to deposit metal on the printed structure, and laser ablation. Once manufactured the sensors can be sampled directly from a microcontroller with only the use of an external pull-down resistor. Finally, sensors are subjected to an external airflow to capture information on various flow gusts.

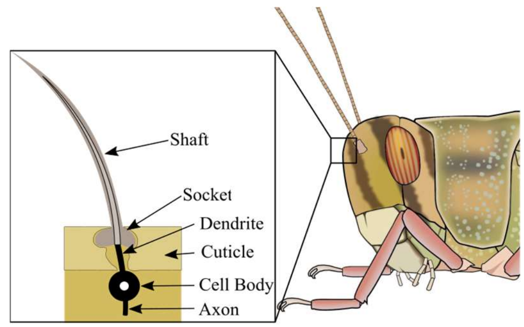

Figure 1: Desert Locust Schistocerca gregaria head with a cross section of a setae.

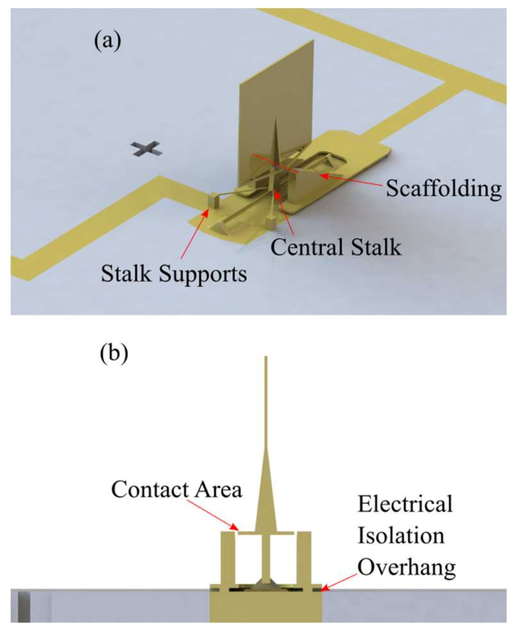

Figure 2: (a) An isometric view of a sensor with major design components highlighted. (b) Cross section of sensor with ohmic contacts and electrical isolations highlighted.

SENSOR DESIGN AND FABRICATION

Mechanical Design

The airflow sensor is composed of two isolated bodies, a central stalk, and an external scaffolding (Fig. 2a). When the sensor experiences an external flow that surpasses the designed threshold, the stalk will deflect to the point of initiating ohmic contact with the scaffolding, completing the circuit.

Previous work from some of the authors used a similar approach to develop switch-based strain sensors. This work builds on this concept and applies it to flow detection [7]. The flow sensor achieves similar sensing by employing a large displacement torsional spring. This rotational joint is designed to be robust but also compliant enough to produce efficient angular displacement to result in ohmic contact [8]. The torsional spring is also adapted from previous work [9]. To electrically isolate the stalk from the outer scaffolding, a series of large overhanging structures were utilized [10] (Fig. 2b). These overhangs act as a shadow mask during the sputtering process allowing components to be electrically isolated.

Modeling and Sensor Parameters

An analytical model was created that relates the geometric parameters of a sensor to its expected deflection under a particular flow. This model calculates the total linear displacement of the ohmic contact faces, or sensor gap, that is achievable for any geometric configuration. The general form of this equation accounts for torsional and bending displacement in the spring, and is shown as Eqn. 1 below. Eqns. 2-7 use the defined parameters from Table 1 and Fig. 3 to define both displacements. The values shown in Table 1 were used in a sensor designed for 4 m/s flow detection.

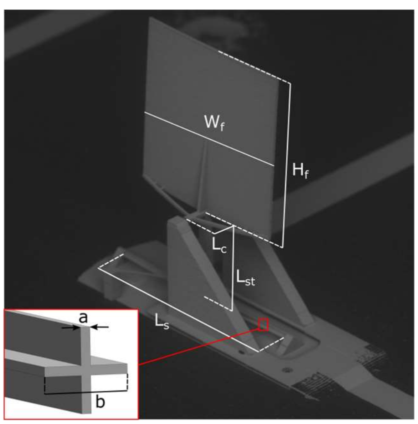

Figure 3: Isometric view of a single flow sensor captured using a scanning electron microscope with highlighted geometric features.

$$G_s = \delta_b + \delta_t \tag{1}$$

$$\delta_b = \frac{F(\frac{L_s}{2})^3}{2EI} \tag{2}$$

$$\delta_t = L_{st}\,sin(\theta) + L_c cos(\theta) - L_c \tag{3}$$

$$F = \rho v^2 2 W_f H_f C_d \tag{4}$$

$$\theta = \frac{LT}{2GJ} \tag{5}$$

$$T = F sin(\theta) L_s \frac{W_f}{2} \tag{6}$$

$$I = \frac{ab^3 + ba^3 - a^4}{12} \tag{7}$$

Two-Photon Polymerization Properties

The fabrication process takes advantage of two-photon polymerization (TPP), a microscale resin 3D printing process. The sensors were fabricated out of IP-S (Nanoscribe), a TPP photoresin. To account for the large suspended structure of the design, a process known as split block modification was utilized. The Describe slicing software (Nanoscribe) splits each model into multiple parts, or blocks, and prints each segment of the model before moving to a new print block. This is due to a limited printing field of 400 µm with the 25x objective. This can result in overhanging structures that can drift during printing. When using large split blocks, the initial layers of these structures are printed and result in a long and thin layer. This layer is liable to drift in the printing resin prior to the next layer being printed, resulting in incomplete torsional springs. To remedy this, each spring was printed with a set of modified blocks [11]. These blocks were printed in segments of 15µm along the length of the spring, creating shorter initial layers, allowing for additional layers to be printed before major drifting occurs.

Table 1: Geometric Parameters for Fabricated Sensors at 4 meters per second airflow

Parameter	Symbol	Value
Spring Length	L_s	500 µm
Stalk Length	L_{st}	200 µm
Contact Length	L_c	120 µm
Fin Width	W_f	750 µm
Fin Height	H_f	750 µm
Ind. Spring Width	a	4 µm
Tot. Spring Width	b	35 µm
IP-S Elastic Modulus	E	5110 MPa

Utilizing small split blocks is beneficial for producing large overhangs, but resulted in a nearly 600% increase in print times. To reduce print times, this work employed a mixture of block sizes allowing for small blocks in the initial layers and large blocks for upper layers. This was achieved by modifying the printer g-code with a custom MATLAB script.

Printing

Flow sensors are printed on a polyethylene terephthalate (PET) substrate with a thin coating of indium tin oxide (ITO) (Fig. 4a). These substrates were cut from a 7-mil thick film of ITO-coated PET using a LPKF ProtoLaser U4 (LPKF) [12]. This substrate was mounted to a thin glass wafer prior to printing. The 3D print was then aligned using laser cut fiducials, and the sensors were directly printed on the substrate by TPP with a Nanoscribe Photonic Professional GT+ (Nanoscribe) utilizing Dip-In Laser Lithography (DiLL) mode and a negative photoresist (IP-S, Nanoscribe) [11]. In this work, all samples were printed with a 25X/NA 0.8 objective (Zeiss) at a laser power and scanning speed of 50 mW and 100,000 µm/s respectively. The laser power was reduced to 35mW for the first 10 base layers to reduce bubbling at the substrate. The slicing and hatching distances used were 1 µm and 0.5 µm, respectively. Once printed, the structures were developed in propylene glycol methyl ether acetate (PGMEA, Sigma-Aldrich) for 20 minutes, then immersed in isopropyl alcohol (IPA) for 2 minutes to wash away any remaining developer and photoresist. The sensors were then left in the air to dry prior to sputter deposition.

Conductivity and Electrical Isolation

After drying, the substrates were removed from the glass slide and a 75nm layer of gold was applied with sputter deposition (Perkin Elmer, 2400-6J) to provide electrical conductivity (Fig. 4b).

After deposition, each sensor was electrically connected to the other sensors in the array. To achieve electrical isolation, excess gold was removed from the substrate through laser ablation using an LPKF ProtoLaser U4. To avoid destroying sensors due to the laser head movement and excessive airflow, the substrate was placed face

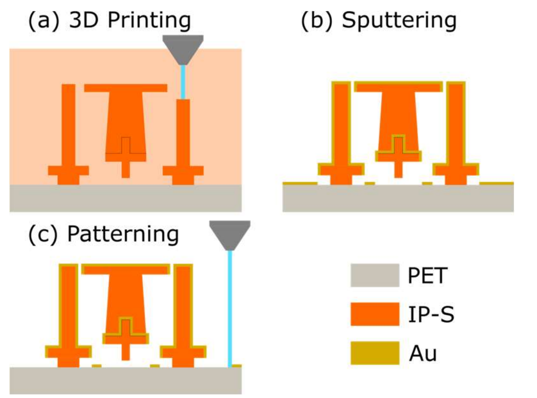

Figure 4: Sensor Fabrication process: (a) Desired structures are 3D printed on PET substrate using TPP. (b) Sputter deposition of gold conductive layer. (c) Laser ablation for electrical isolation.

down leaving the samples suspended through an opening in the LPKF air permeable pad. This technique was developed to ablate the gold by focusing the laser through the substrate, allowing for ablation on the surface facing away from the laser head without damaging the substrate. Additionally, the large distances between each sensor in the array magnified alignment errors during ablation. The fiducials did not provide accurate alignment alone; thus, an alignment calibration was done. A series of printed crosses was used for this additional alignment, after which the gold was ablated (Fig. 4c). The final step in sensor manufacturing was to remove the stalk support structure manually with a probe station.

EXPERIMENTAL METHODS

The experimental setup for electrical isolation testing of these sensors is shown in Fig. 5a. The resistivity of the sensor was measured under a probe station (S-250-6, Signatone) with tungsten needles and was connected to a source measure unit (Keithley) to measure two wire resistance through the sensors. A third probe was then utilized to actuate the sensors by manually closing them. In this way the open and closed resistance could be measured for individual sensors.

Fig. 5b shows an experimental setup for gust detection. The sample was attached to a glass slide, and a circuit board was adhered to the sensor pads on the substrate with an anisotropic conductive adhesive film (3M). Each sensor scaffolding was then connected to the 5V pin on an Arduino Nano Every (Arduino), and each stalk was connected to an individual interrupt pin. Each interrupt pin was coupled with an external pull-down resistor. When the switch was open a low voltage state was observed by the digital pin. However, when the flow threshold was reached the switch would close and a high state was seen by the pin. The glass slide was then placed in a holder, and a hair dryer was utilized to produce wind gusts. The velocity of these gusts was measured by a hot-wire anemometer to compare to sensor values. When a sensor in the array was actuated, the sensor activation was captured on the Arduino and the Boolean pin value was printed to the serial monitor, indicating that a flow was detected.

RESULTS

This work was able to produce low latency mechanosensors for airflow detection. These sensors are quick to fabricate and do not require an etching process to create the large overhanging structures present in the design. With the advancements in split block splicing and laser ablation, a full array of sensors can be fabricated in less than a day. One set of sensors produced was optimized for 0.5 m/s

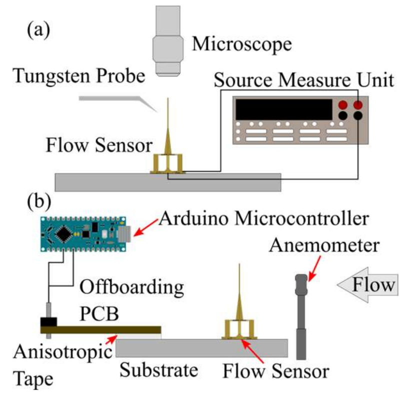

Figure 5: (a) Experimental setup for electrical isolation testing. (b) Experimental setup for gust detection of flow sensors.

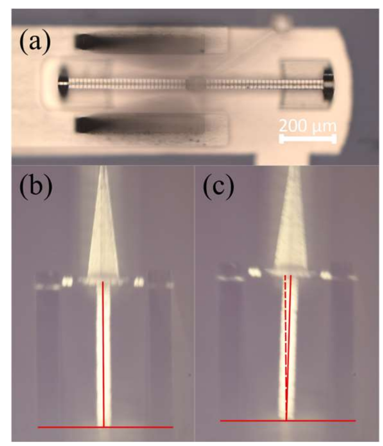

Figure 6: (a) Top view of torsional spring highlighting small split blocks (b) Side view of sensor at resting state on probe station. (c) Side view of sensor in actuated state on probe station

gusts; a flow of 0.5 m/s caused a nearly pure rotational displacement of 1.75 degrees to close the 12 µm sensor gap (Fig. 6).

This work realized the fabrication of a sensor that was consistently capable of detecting 0.5 m/s gusts. Fig. 7 shows detection data from a single sensor in an array. The 0.5 m/s sensor was subjected to two different flow velocities, one measuring roughly 0.5 m/s according to a hot wire anemometer, and one measuring roughly 1 m/s. These flows can be differentiated in the data itself by the frequency through which the signals oscillate. It was observed with a microscope that airflow resulted in sensor oscillation rather than a quasistatic sensor rotation. While the sensor does deflect rotationally and contact the outer scaffolding, it was found that the higher the velocity, the more side to side oscillations are observed in the fin, and transversely in the contact surfaces. This oscillation results in a higher frequency of sensor impulses, rather than simply connecting the circuit and remaining connected. This phenomenon is beneficial in airflow detection, as it could be utilized to estimate the wind velocity. By arraying these sensors and measuring the time between sensor activation, it is possible to calculate the flow velocity of a gust across the sensors. One downside is that once the sensors have been activated and continue to remain active, time dependent data can no longer be analyzed, and the sensors can only indicate that a gust is being experienced at a higher velocity than the flow threshold.

Investigation into this oscillation effect may result in additional information by mapping the frequency to airflow. This is a promising revelation, as the setae of desert locusts naturally oscillate as well. Locusts send neural spikes to the insect's flight motor

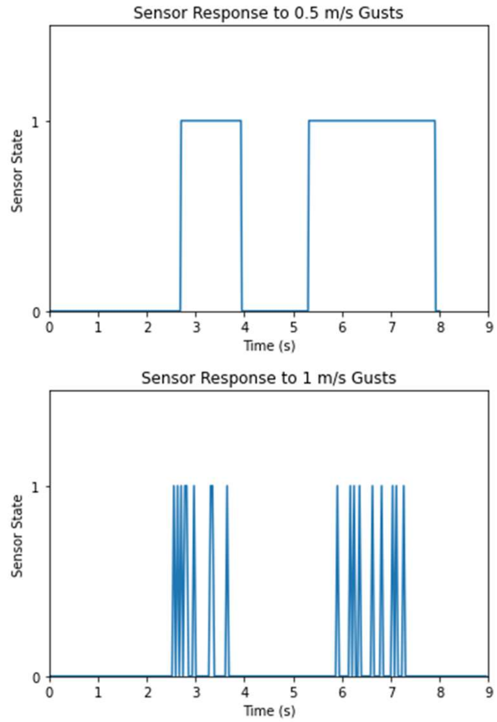

Figure 7: Sensor response to a 0.5 m/s and 1.0 m/s flow velocity These sensors were designed to detect 0.5 m/s gusts. Sensor oscillation is observed at the higher flow velocity

neurons to direct the wing movement similar to how these sensors send a single simulated neural spike to the microcontroller. However, locusts also utilize their setae after a gust has been detected by allowing them to oscillate in the wind. The frequency of these oscillations is filtered within the neural pathways of the insect and relayed to the flight motor neurons as well, continuously updating the insect on the external flow. These oscillations were found to change with flow velocity and were also dependent on the type of setae that was activated, as setae have different flow thresholds [4]. By replicating this result and producing simulated neural spikes these sensors more closely resemble the ones found in nature than other MEMS airflow sensors. For example, a sensor produced at a similar scale that utilizes the change of wire resistance due to strain [6], was experimented with air velocities between 0 and 45 m/s. In these tests, the lowest experimental velocity used to find a change in resistance was just above 5 m/s. This indicates that the sensors developed in this process can detect a flow velocity at an order of magnitude less than other designed MEMS airflow sensors.

CONCLUSIONS

A rapid fabrication process that employs 3D printing, metal sputter deposition and laser ablation was built upon in this work to present a microscale flow sensor and its design process. The fabrication addressed the 3D printing of long, unsupported overhangs and, using these fabrication techniques, produced a highly sensitive threshold-based flow sensor. These sensors demonstrated a high selectivity to low flow velocities, and produced impulse signals like the neural spikes observed in locusts. These impulses can be detected by the systems on a MAV without the need for resource intensive monitoring, filtering, or amplification.

This work provides a foundation for the further development of these flow sensors for use within micro robotics and MAVs. This design can be adapted to different flow thresholds, and can be utilized in arrays for omni-directional detection. Using these arrays, the flow velocity and direction can also be characterized. Future efforts will be focused on the implementation of these sensors in an array, and the characterization of flow velocity versus sensor oscillation. Additionally, the developed techniques can be used to manufacture a sensor with a series of stacked torsional springs, resulting in a single sensor used for omnidirectional flow detection, further decreasing the sensor package size.

ACKNOWLEDGEMENTS

The authors would like to thank the staffs of the Clair and John Bertucci Nanotechnology Laboratory and Soft Lithography Lab at Carnegie Mellon University for their assistance in the microfabrication and 3D printing of these devices. The authors would also like to thank Sukjun Kim for his help and advice. This research effort was supported by the Air Force Office of Scientific Research (AFOSR) MURI award number FA9550-19-1-0386.

REFERENCES

[1] B. Pratt, et al., “Neural evidence supports a dual sensory-motor role for insect wings”, *Proceedings of the Royal Society Biological Sciences,* 234, (2017).

[2] J. M. Camhi, “Locust wind receptors: U. transducer mechanics and sensory response”, *Journal of Experimental Biology,* 50, 335-348 (1969)

[3] D. M. Guthrie, “Observations on the nervous system of the flight apparatus in the locust Schistocerca Gregaria”, *Journal of Cell Science,* 105, 183-210 (1964)

[4] J. M. Camhi, “Locust wind receptors: II. Interneurons in the cervical connective”, *Journal of Experimental Biology,* 50, 349-362 (1969)

[5] G. M. Gremillion, et al., “Disturbance rejection with distributed acceleration sensing for small unmanned aircraft systems”, *American Institute of Aeronautics and Astronautics,* 50(8), 2233-2246 (2016)

[6] Y. Wang, et al., “A mems-based air flow sensor with a free-standing microcantilever structure”, *Sensors,* 7(10), 2389-2401 (2007)

[7] R. Kubicek, et al., “Rapid prototyping of 3d printed mems arrays on flexible substrates”, *Solid-State Sensors, Actuators and Microsystems Workshop* (2022)

[8] Y. Moon, et al., “Design of large-displacement compliant joints”, *Journal of Mechanical Design*, 127(4), 2389-2401 (2002)

[9] S. Kim, et al., “Fabrication and characterization of 3d printed out-of-plane torsional comb-drive actuators for microrobotics”, *21st International conference on Solid-State Sensors, Actuators and Microsystems (Transducers),* 6-9 (2021)

[10] S. Kim, et al., “A two-step fabrication method for 3d printed microactuators: Characterization and actuated mechanisms.” *Journal of Microelectromechanical Systems,* 29(4) 544-552 (2020)

[11] D. E. Marschner, et al., “A methodology for two-photon polymerization micro 3d printing of objects with long overhanging structures”. *Additive Manufacturing,* 66 (2022)

[12] R. Kubicek, et al, “Keeping it Simple: Bio-Inspired Threshold-Based Strain Sensing for Micro-Aerial Vehicles” *2021 IEEE/RSJ International Conference on Intelligent Robots and Systems,* pp. 7505-7511, (2021)

CONTACT

B. Miller, b.miller1199@gmail.com